Inorganic Chemistry

Article

pubs.acs.org/IC

Zero-Field Splitting in Pseudotetrahedral Co(II) Complexes: a Magnetic, High-Frequency and -Field EPR, and Computational Study

Monika Idešicová,[†] Ján Titiš,[†,*] J. Krzystek,[‡,*] and Roman Boča[†]

[†]Department of Chemistry (FPV), University of SS. Cyril and Methodius, SK-917 01 Trnava, Slovakia

[‡]National High Magnetic Field Laboratory, Florida State University, Tallahassee, Florida 32310, United States

Supporting Information

ABSTRACT: Six pseudotetrahedral cobalt(II) complexes of the type $[CoL_2Cl_2]$, with L = heterocyclic N-donor ligand, have been studied in parallel by magnetometry, and high-frequency and -field electron paramagnetic resonance (HFEPR). HFEPR powder spectra were recorded in a 50 GHz < ν < 700 GHz range in a 17 T superconducting and 25 T resistive magnet, which allowed constructing of resonance field vs frequency diagrams from which the fitting procedure yielded the $S = 3/2$ spin ground state Hamiltonian parameters. The sign of the axial anisotropy parameter D was determined unambiguously; the values range between −8 and +11 cm^{-1} for the given series of complexes. These data agree well with magnetometric analysis. Finally, quantum chemical *ab initio* calculations were performed on the whole series of complexes to probe the relationship between the magnetic anisotropy, electronic, and geometric structure.

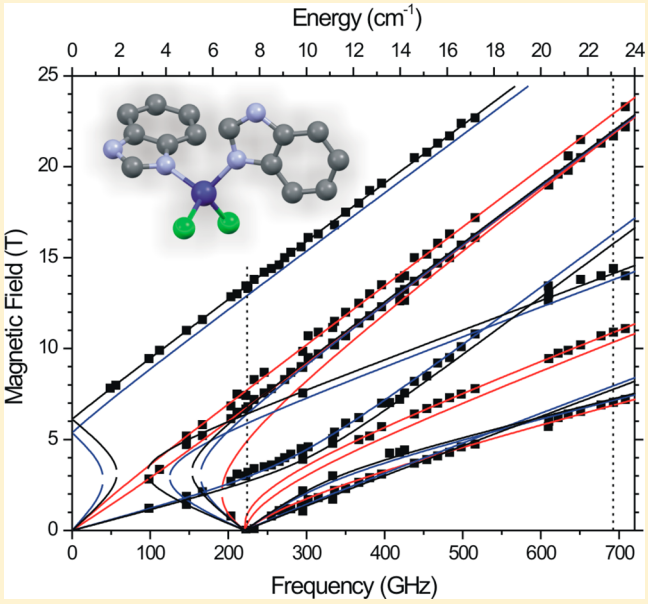

INTRODUCTION

A magnetostructural correlation is defined as a relationship between the magnetic and structural parameters of a molecular entity. Such correlations have been investigated intensively over recent decades. Initially, they involved the correlation of the exchange coupling constant J in binuclear Cu(II) complexes vs the Cu−O−Cu angle in the superexchange path.[1] In addition to collecting the relevant data and formulating empirical correlations, a theoretical analysis was often attempted based upon density functional theory.[2] Such correlations were also extended to atoms other than copper.[3] For instance, Gorun and Lippard proposed a correlation J vs p, where p is the shortest of the Fe−O contacts within the superexchange path in binuclear Fe(III) complexes; this correlation follows a decreasing exponential.[3a] This type of correlation could be termed as J correlations in order to distinguish them from the more recently proposed magnetostructural D correlations. In the latter case, the axial zero-field splitting (zfs) parameter D (or more specifically D_{mag}) was correlated with the structural tetragonality parameter D_{str} in a series of hexacoordinate Ni(II) complexes.[4] In this case the correlation is represented by a straight line (in fact by two, nearly collinear, straight lines) for a geometry of compressed/elongated tetragonal bipyramid keeping D_{4h} symmetry. It was found that this correlation possesses a predictive character.[4c] In hexacoordinate Co(II) complexes, however, the magnetostructural D correlation no longer follows a straight line: it is defined by a number of nonlinear curves in the segment of compressed tetragonal bipyramids.[5] This can be rationalized by inspecting the energy gap Δ_{cfm} between the ground and the first excited crystal-field multiplets (Γ_6, Γ_7) as modeled within and beyond the spin-Hamiltonian formalism.[6] The D values for hexacoordinate Co(II) can be as large as 100 cm^{-1} or more, which allows their detection by common FAR-IR spectrometers.[7]

Pseudotetrahedral Co(II) complexes are interesting high-spin systems, not least in light of the recent discovery of single-molecule magnetism in mononuclear Co(II) complexes.[8a,d] Although high-spin Co(II) does not appear in biologically active systems, it has been often substituted for a "spectroscopically-silent" Zn(II) ion in proteins.[8b] In a high-spin Co(II) ion, the ground crystal-field term $^4A_2(T_d)$ is split into two multiplets (each referring to a Kramers doublet Γ_6 and Γ_7) separated by $\Delta_{cfm} = 2(D^2 + 3E^2)^{1/2} \sim 2D$.[8c−e] Tetrahedral ligand environment produces a rather weak crystal field so that the excited terms are relatively low-lying in pseudotetrahedral

Received: April 19, 2013
Published: August 7, 2013

   dx.doi.org/10.1021/ic400980b | *Inorg. Chem.* 2013, 52, 9409−9417

systems. Therefore, the enhanced second-order perturbation of the ground crystal-field term generates significant D values that, in the exceptional cases for Co(II), can approach values of 70 cm^{-1} [8d,9] but in most cases are lower, on the order of 2−20 cm^{-1}. For comparison, in hexacoordinate Ni(II) complexes, $|D|$ is typically <10 cm^{-1} despite the fact that the spin−orbit splitting parameter ($\lambda = \pm \xi/2S$) for Ni(II) is much larger than the parameter for Co(II): $\lambda(Ni^{II}) = -315$ cm^{-1}, $\lambda(Co^{II}) = -172$ cm^{-1}.[6]

Structural and magnetic data relevant to a novel magneto-structural D correlation for pseudotetrahedral Co(II) complexes have begun to accumulate.[10] However, the situation is more complex than in Ni(II), since in pseudotetrahedral complexes of the $[CoL_4]$ and $[CoL_2X_2]$ type, the distortions from ideal tetrahedron are more variable, and D_{2d}, C_{2v}, C_2, and C_1 symmetries often occur. The second complication arises from the fact that the susceptibility data for pseudotetrahedral Co(II) complexes are insensitive to the sign of the D parameter. This effect is demonstrated in Figure S1 in the Supporting Information, where a calculated temperature dependence of the effective magnetic moment (or alternatively the product function χT) is displayed for positive and negative D parameters for different spin states: for $S = 3/2$, both curves are identical. Therefore, it is difficult or even impossible to assign the sign of the D parameter from the powder susceptibility data for $S = 3/2$ systems alone. Single-crystal data, on the other hand, are in principle capable of distinguishing the sign of the D parameter.[11,12] A field dependence of magnetization (Figure S1, bottom) provides a slightly better resolution, since at high fields the D sign separates the individual curves reliably. For Co(II) complexes, a simultaneous treatment of the powder susceptibility and magnetization data is therefore the only possible way to determine the complete zfs parameters from magnetometry alone. However, such results still cannot be taken as definitive when $|D/hc| < 3$ cm^{-1}, or particularly when the rhombic zfs term E/D is nonzero.

The need to obtain highly reliable zfs data for magneto-structural correlations motivated us to conduct a parallel investigation of a series of $\{Co(II)N_2Cl_2\}$ complexes by magnetometry and high-frequency and -field electron paramagnetic resonance (HFEPR). The former includes a temperature dependence of the isofield magnetic susceptibility and a field dependence of the isothermal magnetization. The latter involves recording multifrequency (~50−700 GHz) EPR spectra in magnetic fields up to 25 T. HFEPR is necessary for a definitive determination of the complete zfs tensor in $S = 3/2$ systems with large zfs because conventional EPR is typically not of sufficient frequency to detect the inter-Kramers transitions, as previously demonstrated in the case of pseudotetrahedral Co(II) complexes.[13] Instrumental progress in this field has led to increasingly sophisticated investigations by combined experimental techniques and quantum-chemical calculations over the years.[8c,e,14]

EXPERIMENTAL SECTION

Synthesis and Structure Determination. A series of Co(II) complexes of the $[CoL_2Cl_2]$ type was prepared and studied, where in **1**, L = 1,2-dimethyl-5-nitroimizadole; **2**, L = 2-aminopyrimidine; **3**, L = benzimidazole; **4**, L = cytosine; **5**, L = imidazole; and **6**, L = quinoline (see Figure 1).

Details of the synthesis of complexes **1**−**3** were already published.[9] The remaining complexes (**4**−**6**) were prepared by a similar recipe: a solution of 0.1 mmol of $CoCl_2 \cdot 6H_2O$ in 10 mL of ethanol was added to a solution of 0.2 mmol of the ligand in 15 mL of ethanol under intense stirring (the molar ratio L/Co = 2:1). The two solutions were refluxed for 1 h. Deep blue crystals were obtained by slow evaporation of the solution at room temperature. Anal. Calcd for **4**, $C_8H_{10}N_6O_2CoCl_2$ (M = 352.04): C, 27.3; H, 2.86; N, 23.9. Found: C, 26.6; H, 2.98; N, 23.6. Anal. Calcd for **5**, $C_6H_8N_4CoCl_2$ (M = 266.00): C, 27.1; H, 3.03; N, 21.1. Found: C, 26.5; H, 3.16; N, 20.1. Anal. Calcd for **6**, $C_{18}H_{14}N_2CoCl_2$ (M = 388.16): C, 55.7; H, 3.64; N, 7.22. Found: C, 55.6 H, 3.77; N, 7.30.

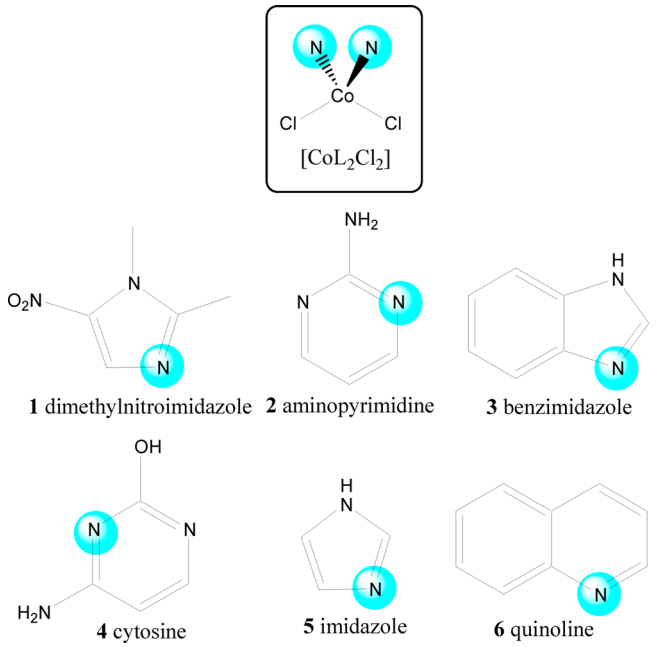

Figure 1. A general molecular structure of the complexes under study and those of the ligands. The donor nitrogen atoms are highlighted.

All complexes have been already structurally characterized,[15] and the corresponding data can be retrieved from the Cambridge Crystallographic Data Centre.[16] Molecular structures of the complexes under study are displayed in the Supporting Information (Figure S3).

Magnetic Measurements. Magnetic data were taken with the SQUID apparatus (MPMS-XL7, Quantum Design) equipped with a B = 7 T superconducting magnet. The susceptibility was taken in the RSO mode of detection at B = 0.1 T; it was corrected for the underlying diamagnetism and converted to the effective magnetic moment. The isothermal magnetization has been measured at two temperatures: T = 2.0 and T = 4.6 K. The data analysis was done using the POLYMAGNET program package.[17a]

HFEPR Measurements. HFEPR data were acquired using either of two facilities. The EMR Facility includes a spectrometer described elsewhere,[18a] modified by the use of Virginia Diodes Inc. (VDI) sources, operating in a 50−420 GHz frequency range. The spectrometer is associated with a 17-T superconducting magnet. The DC Facility includes a setup[18b] using tunable sources (backward wave oscillators), operating in a 100−700 GHz frequency range, associated with the 25-T resistive Bitter-type "Keck" magnet. The samples were either used "as is" after initial crystallization, finely ground, or eventually pressed into pellets with n-eicosane. Approximately 50−100 mg of material was used in each case. The data analysis was done using the SPIN program.[17b]

Quantum-Chemical Calculations. Theoretical calculations of the zfs based on X-ray diffraction-determined structures were performed with the ORCA program.[19a] For this purpose, an *ab initio* wave function based method has been chosen, such as complete active space self-consistent field (CASSCF) improved with the second-order N-electron valence perturbation theory (NEVPT2).[19b−e] An active space in which seven electrons are distributed into the five cobalt d orbitals (CAS(7,5)) was employed along with the TZVP basis set for all

dx.doi.org/10.1021/ic400980b | Inorg. Chem. 2013, 52, 9409−9417

Table 1. Bond Distances (Å) and Bond Angles (deg) for the Co(II) Complexes

no.	symm.	d_{Co-N}	d_{Co-Cl}	α	β	τ_1, τ_1'	τ_2, τ_2'
1	C_2	2.034(2×)	2.231(2×)	102.44	111.02	120.9(2×)	101.3(2×)
2	C_2	2.041(2×)	2.243(2×)	114.47	110.42	108.4(2×)	107.6(2×)
3	C_1	2.004	2.241	106.22	111.95	109.1	111.2
		2.010	2.254			107.6	110.6
4	C_1	2.053	2.296	110.36	103.40	113.9	104.8
		2.057	2.303			112.4	111.6
5	C_1	1.989	2.238	105.34	111.18	105.3	115.2
		1.998	2.263			107.9	111.9
6	C_2	2.070(2×)	2.244(2×)	107.17	113.44	102.6(2×)	115.7(2×)

elements. In the CASSCF procedure, the orbitals were optimized for the average of 10 quartet (^{4}F and ^{4}P terms of the free Co(II)) and 28 doublet (^{2}G, ^{2}H, ^{2}P, and ^{2}D terms) roots. Taking into account the size of some ligands, seven roots of the ^{2}F term were excluded mainly to speed up the calculations. The benchmark calculation showed that an inclusion of the given terms improves the results by only about 2%.

The state-averaged (SA) CASSCF calculations were performed on top of quasi-restricted DFT/BP86/TZVP orbitals. The D values were calculated through quasi-degenerate perturbation theory (QDPT) in which the spin−orbit coupling operator (in SOMF approximation)[19f] is diagonalized in the basis of the nonrelativistic SA-CASSCF/NEVPT2 eigenfunctions.[19g] Diagonalization of the resulting matrix yields the energy levels and eigenvectors of the coupled states that were used for constructing the D tensor through the formalism based on second-order perturbation theory.[19h]

RESULTS AND DISCUSSION

Molecular Structures. Bond distances and bond angles relevant for the studied complexes are presented in Table 1. In all cases, the chromophore $\{CoN_2Cl_2\}$ refers to a distorted tetrahedron. As expected, Co−Cl distances are longer (2.23−2.30 Å) than Co−N distances (2.00−2.07 Å). The six bond angles within the chromophore are variable and can be classified according to Figure 2: N−Co−N angle α, Cl−Co−Cl angle β, and four N−Co−Cl angles τ.

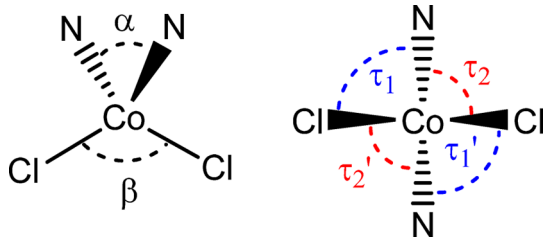

Figure 2. Labeling of bond angles in the $\{CoN_2Cl_2\}$ chromophore.

The highest possible symmetry for a $\{CoN_2Cl_2\}$ chromophore is C_{2v} for which $\tau_1 = \tau_1' = \tau_2 = \tau_2'$ (variation of α and β does not change this symmetry). However, as it can be seen from Table 1, we are dealing with lower symmetries than C_{2v} since (i) for **1**, **2**, and **6** $\tau_1 = \tau_1' \neq \tau_2 = \tau_2'$ and (ii) for **3**, **4**, and **5**, we have $\tau_1 \neq \tau_1' \neq \tau_2 \neq \tau_2'$. The complexes, therefore, belong to C_2 and C_1 point groups, respectively.

Magnetometry. At room temperature all complexes show an effective magnetic moment $\mu_{eff} \approx 4.6\ \mu_B$. This value stays constant down to 10−15 K when it drops to $\mu_{eff} \approx 3$−$3.5\ \mu_B$ at $T = 1.9$ K as an effect of zfs. The magnetization per formula unit $M_1 = M_{mol}/N_A$ saturates to the values of $M_1 \approx 2.6$−$3.1\ \mu_B$ at $T = 2.0$ K and $B = 7.0$ T; these values are consistent with the $S = 3/2$ state characterized by sizable zfs. The temperature dependence of the magnetic susceptibility converted to an effective magnetic moment, and the field dependences of the magnetization for complex **1** are shown in Figure 3; magnetic results for all complexes are displayed in Figure S2.

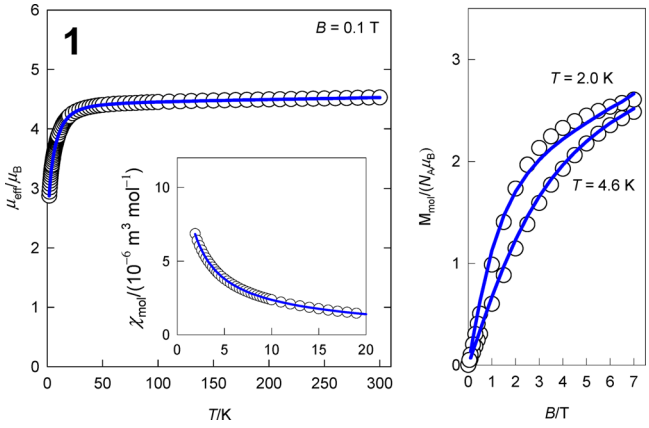

Figure 3. Magnetic data for complex **1** (circles, experimental; lines, simulated, based on best-fit parameters as listed in Table 2). $R(\chi) = 0.0038$, $R(M) = 0.0312$.

Magnetic data were fitted with the usual spin Hamiltonian where the axial zfs parameter D and the rhombic parameter E occur (for details, see the Supporting Information)

$$\hat{H}_{k,l} = D(\hat{S}_z^2 - \vec{S}^2/3)\hbar^{-2} + E(\hat{S}_x^2 - \hat{S}_y^2)\hbar^{-2} + \mu_B B_m(g_x \sin\vartheta_k \cos\varphi_l \hat{S}_x + g_y \sin\vartheta_k \sin\varphi_l \hat{S}_y + g_z \cos\vartheta_k \hat{S}_z)\hbar^{-1} \quad (1)$$

The generated energy levels enter the formulas of the statistical thermodynamic allowing reconstruction of the susceptibility and magnetization for the trial set of magnetic parameters.[12] The Zeeman term has been averaged over 210 points distributed uniformly over one hemisphere giving rise to a correct powder average. Two additional corrections were applied to the susceptibility data: the (zj) parameter describes an effective molecular field, and χ_{TIM} is the temperature-independent magnetism (this takes into account uncompensated diamagnetism, temperature-independent paramagnetism, and the response of the sample holder). The fitting procedure is based upon minimization of the error functional constructed as a product of the relative errors for the susceptibility and magnetization: $F_1 = R(\chi) \times R(M)$. Alternatively, a weighted sum has also been applied: $F_2 = w_1R(\chi) + w_2R(M)$. The resulting spin Hamiltonian parameters (g, D, and E) are listed in Table 2 along with those determined previously by magnetometry for complexes **1**−**3** (where the parameter E

dx.doi.org/10.1021/ic400980b | Inorg. Chem. 2013, 52, 9409−9417

Table 2. $S = 3/2$ Spin Hamiltonian Parameters of the Co(II) Complexes[a]

complex	method	g_z	g_x, g_y	$(D/hc)/cm^{-1}$	$(\lvert E\rvert/hc)/cm^{-1}$	$\lvert E/D\rvert$
1	Mag[b]	2.163	2.350	+11.40		
	Mag[c]	2.115	2.240, 2.515	+11.13	0.11	0.01
	HFEPR	2.16(1)	2.37(1), 2.09(2)	+11.38(5)	2.36(1)	0.21
	QCC			±15.30[d]		0.30
2	Mag[b]	2.161	2.302	+12.20		
	Mag[c]	2.362	2.193, 2.197	−9.99	2.40	0.24
	HFEPR	2.220(6)	2.246(5), 2.225(15)	−7.99(1)	2.23(1)	0.28
	QCC			−9.96		0.16
3	Mag[b]	g_{iso} 2.290		−3.15		
	Mag[c]	2.304	2.529, 2.415	+2.18	0.50	0.22
	HFEPR	2.236(2)	2.221(1), 2.24(1)	±3.33[d]	0.93	0.28
	QCC			+4.93		0.20
4	Mag	2.248	2.173, 2.201	−5.23	0.51	0.10
	HFEPR	2.253(6)	2.233(5), 2.220(3)	−4.31(1)	0.23(7)	0.05
	QCC			−6.51		0.12
5	Mag	2.079	2.335, 2.270	+5.67	0.30	0.05
	HFEPR	g_{iso} 2.450		+9.15	1.00	0.10
	QCC			+8.26		0.21
6	Mag	2.496	2.075, 2.113	−6.35	0.03	~0
	HFEPR	2.194	2.210, 2.200	−5.88	1.54	0.26
	QCC			−6.92		0.05

[a]Abbreviations: Mag, Magnetometry; HFEPR, High-Frequency and -Field Electron Paramagnetic Resonance; QCC, Quantum-Chemical Calculation. [b]Magnetic data published previously.[10] [c]New fit parameter sets taking into account rhombic contributions. [d]Sign of D impossible to determine due to a very high rhombicity of the zfs tensor.

was ignored).[10] The complete set of the magnetic parameters is listed in Table S1 in the Supporting Information.

HFEPR. All six complexes delivered a strong HFEPR response at low temperatures (standard measurement temperature was 4.2 or 10 K). In each case, at least one turning point belonging to an inter-Kramers transition was observed and followed through a range of frequencies. This, together with the observation of the zero-field frequency representing the energy gap Δ between the $M_S = \pm 1/2$ and $\pm 3/2$ doublets, made it possible to definitely determine the zfs parameters. However, individual EPR responses of particular complexes differed strongly between them, making it necessary to briefly discuss each complex separately.

Complex **1** measured as a loose sample produced HFEPR resonances (not shown) that clearly displayed field-torquing effects. Grinding and pressing the sample into a pellet improved the quality of the spectra which could be interpreted and simulated (see Figure S4 in the SI). Extending the range of frequencies up to 700 GHz (Figure 4) allowed us to pinpoint the zero-field resonance, which lies just above 720 GHz, allowing us to estimate the parameter $\Delta = 2(D^2 + 3E^2)^{1/2} \sim 24$ cm^{-1} and thus putting a constraint on both D and E values. The spin Hamiltonian parameters were obtained from the 2-D field/frequency map (Figure 5): $|D| = 11.38(5)$ cm^{-1}, $|E| = 2.36(1)$ cm^{-1}, and $\mathbf{g} = [2.37(1), 2.09(2), 2.16(1)]$. As attested by Figures S4 and 4, the sign of D is positive.

Complex **2** as loose powder underwent extreme torquing in the magnetic field so that the resulting spectra could be adequately simulated as for a single crystal (Figure S5). Remarkably, the $M_S = -3/2 \rightarrow +3/2$ transition showed a well-resolved hyperfine structure, particularly at low frequencies and fields (Figure S6). This is a rare event in magnetically undiluted complexes of isotopes possessing nuclear spin, particularly at high frequencies/fields (observations in magnetically diluted systems are more common, and indeed expected[13f]). The structure observed by us consisted of 10 lines, with a coupling constant of approximately 86 mT, and could only be attributed to the ^{59}Co nucleus ($I = 7/2$). The number of components, and the asymmetry of the hyperfine structure, however, made the detailed analysis of the powder spectrum difficult, and we postpone its discussion to a future study of a single crystal since it is not relevant to this work. Complex **2** pressed into a pellet showed completely different spectra that could be well simulated as a powder pattern (Figure S7). Extending the frequency range to 700 GHz, and using the tunable sources (Figure 4), allowed us to fix the zero-field resonance at 530 ± 5 GHz and to estimate the parameter Δ as ~17.7 cm^{-1}. The spin Hamiltonian parameters were obtained from the 2-D field/frequency map (Figure 5): $|D| = 7.99(1)$ cm^{-1}, $|E| = 2.23(1)$ cm^{-1}, $\mathbf{g} = [2.246(5), 2.225(15), 2.220(6)]$. As attested by Figures 4, S5, and S7, the sign of D is negative.

Complex **3** measured as a loose sample produced HFEPR resonances that were both broad and of poorly defined shape (Figure S8). However, a spectrum taken at 222.4 GHz showed a near-zero field transition, allowing us to estimate the parameter Δ as ~7.4 cm^{-1}. Grinding and pressing the sample into a pellet improved somewhat the spectral shape and delivered a more satisfying agreement between experiment and simulation (Figure S9). Finally, extending the range of frequencies up to 700 GHz brought a convincing proof of the accuracy of the spin Hamiltonian parameters, as shown in a 693 GHz spectrum of the pellet (Figure 4). The parameters themselves were obtained from a fit to the 2-D map of turning points (Figure 5): $|D| = 3.33$ cm^{-1}, $|E| = 0.93$ cm^{-1}, $\mathbf{g} = [2.221(1), 2.24(1), 2.236(2)]$. Complex **3** is characterized by a near-maximum rhombicity of the ZFS tensor ($E/D = 0.28$). This plus significant line widths caused many turning points to nearly coincide at a given frequency and made the sign of D both impossible to determine and largely irrelevant.

dx.doi.org/10.1021/ic400980b | Inorg. Chem. 2013, 52, 9409−9417

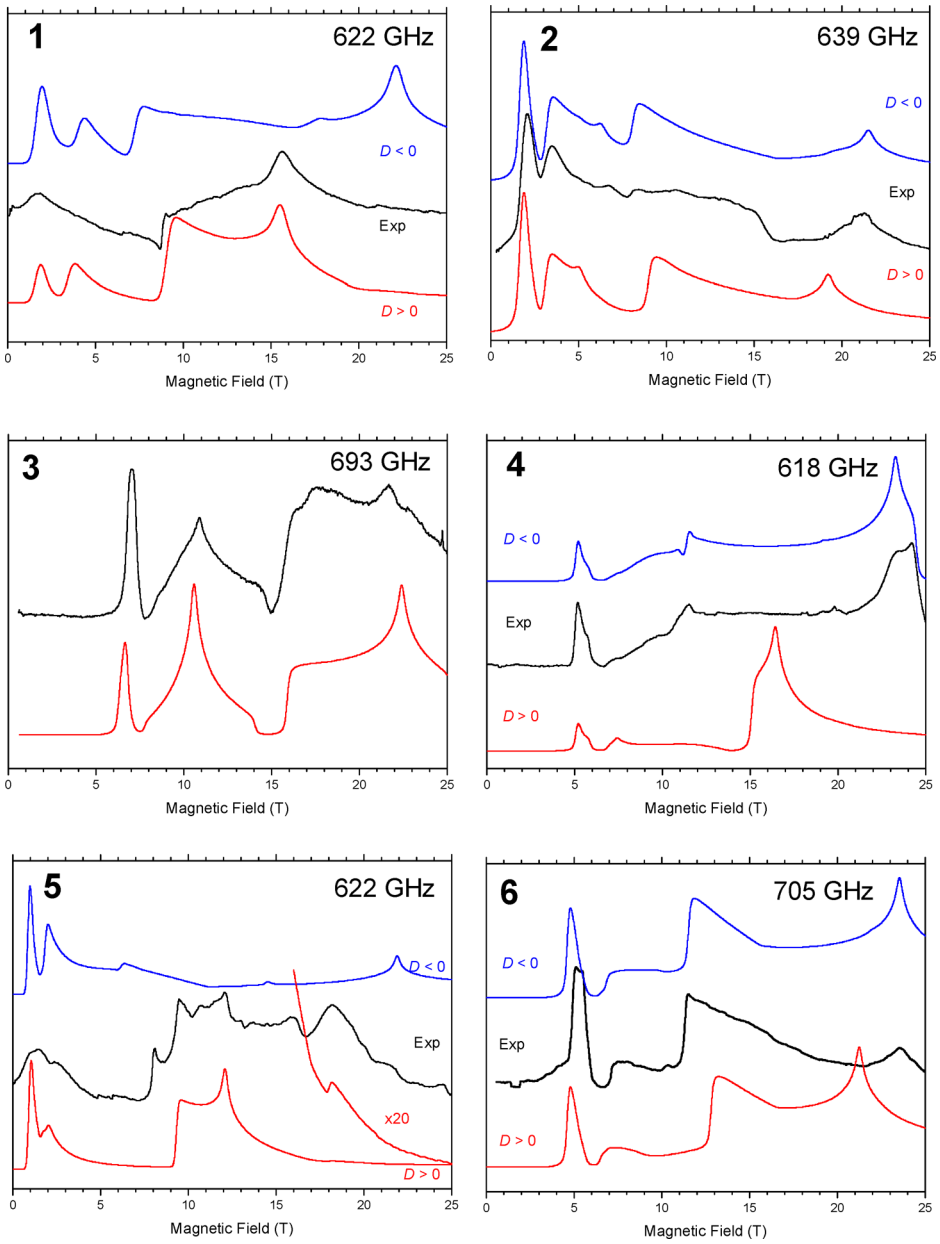

Figure 4. Experimental HFEPR spectra of the complexes studied as pellets at 4.2 K near the top range of frequencies (indicated in each plot) and their simulations assuming a powder distribution of crystallites under the same conditions. The spin Hamiltonian parameters used in the simulations were those obtained from a fit to the 2-D field/frequency map as in Table 2. The submillimeter waves were chopped instead of modulating the magnetic field resulting in absorptive shape. Notes for **3**: The small sharp peak near 25 T belongs to a DPPH marker. Simulation parameters are as in Table 2 except for E that was fixed at the maximum rhombicity condition ($E = 1/3\ D$). Notes for **5**: The spin Hamiltonian parameters used in the simulations were ($|D| = 9.15\ cm^{-1}$, $|E| = 0.93\ cm^{-1}$, and $\mathbf{g} = [2.62, 2.62, 2.45]$. The red trace magnified by a factor of 20 points out a parallel turning point that is prominent in the experiment, but barely visible in the simulation. This illustrates the nonrandom distribution of the crystallites even in a pellet.

Complex **4** was free from field-torquing effects. Consequently, it was not necessary to make a pellet to obtain powder-pattern spectra of excellent quality (Figure S10). The zero-field resonance was observed to lie in the "dead zone" of the VDI source at our disposal, between 224 and 295 GHz. Using the tunable sources (Figure 5), we pinpointed it at 260 ± 5 GHz, allowing us to estimate the parameter $\Delta \sim 8.7\ cm^{-1}$. The spin Hamiltonian parameters were obtained from the 2-D field/frequency map (Figure 5): $|D| = 4.31(1)\ cm^{-1}$, $|E| = 0.23(1)\ cm^{-1}$, $\mathbf{g} = [2.233(5), 2.220(3), 2.253(6)]$. As attested by Figure S10 and particularly Figure 4, the sign of D is negative.

Complex **5** measured as a loose sample produced HFEPR resonances that were uninterpretable, being both broad and of undefined shape (not shown). Grinding and pressing the sample into a pellet only marginally improved the quality of the spectra which still remained uninterpretable at frequencies generated by the VDI source. Extending the range of frequencies up to 700 GHz, however, indicated a zero-field transition appearing at 560 ± 10 GHz, allowing us to estimate the parameter Δ as $\sim 18.7\ cm^{-1}$. Also, high-frequency spectra became interpretable (Figure 4), although the generally poor quality of the spectral data set did not allow us to perform a computer fit as in all the other investigated complexes of the

dx.doi.org/10.1021/ic400980b | Inorg. Chem. 2013, 52, 9409−9417

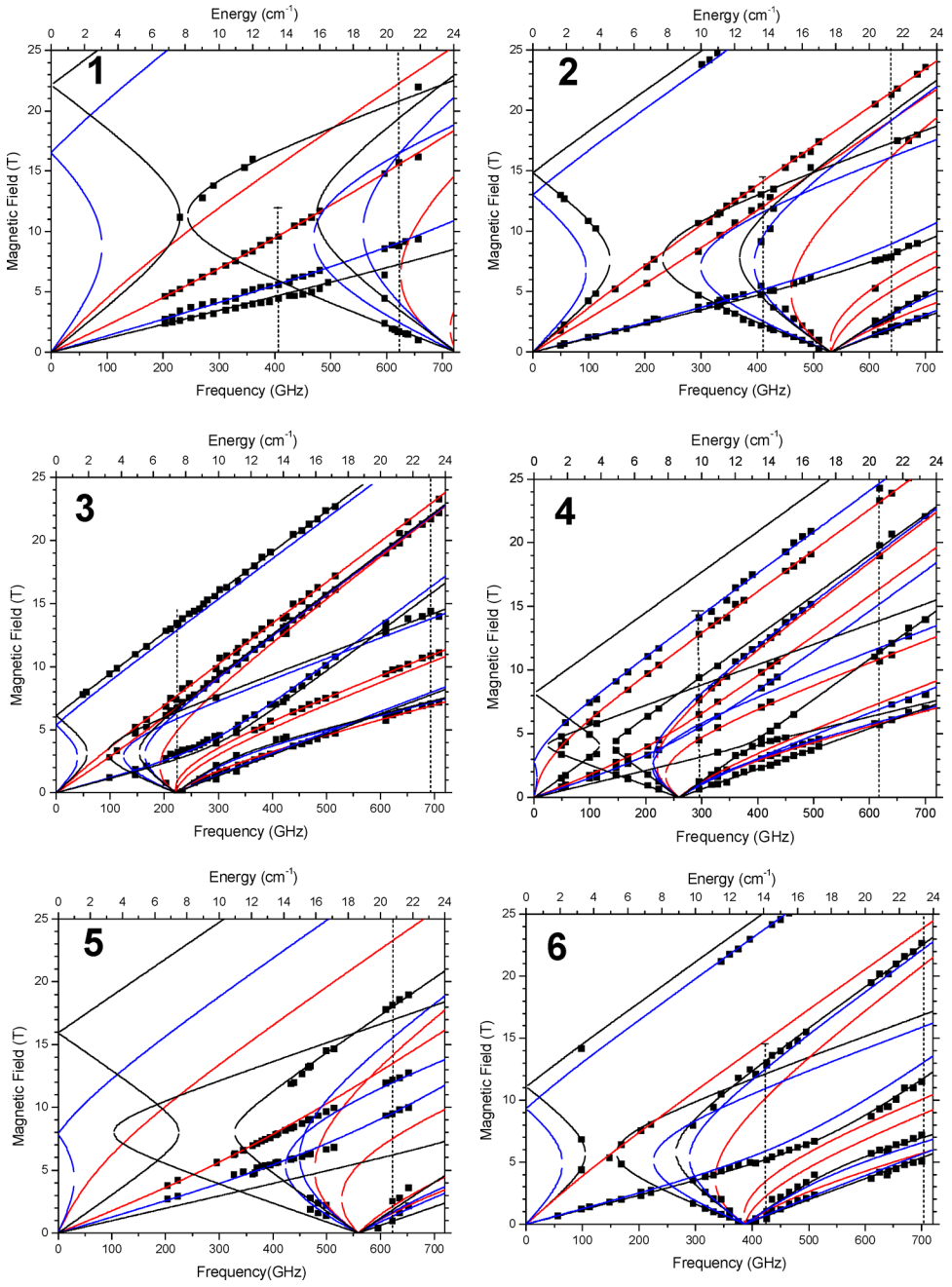

Figure 5. The 2-D maps of turning points in studied complexes as pellets as a function of mm- or submm wave frequency at 4.2−10 K. The squares are experimental points, while the lines were simulated using spin Hamiltonian parameters as in Table 2. Red lines: turning points with $B_0//x$ axis of the ZFS tensor. Blue ines: $B_0//y$ axis. Black lines: $B_0//z$ axis. The dashed lines indicate the frequency and field range of the spectra shown in Figure 4 and Figures S4, S7, S9, S10, and S11, respectively.

series. Figure 5 thus shows our best guess of the field vs frequency dependence, with the parameters: $|D| = 9.15$ cm^{-1}, $|E| = 1.00$ cm^{-1}, and $g = 2.45$ (isotropic). As attested by Figure 4, the sign of D appears positive.

Complex **6** measured as a loose sample produced HFEPR resonances (not shown) that clearly displayed field-torquing effects. They also hinted at the zero-field transition positioned just below 400 GHz. Grinding and pressing the sample into a pellet improved the quality of the spectra which could be interpreted and simulated (Figure S11). Using tunable sources up to 700 GHz (Figure 4) made it possible to more accurately pinpoint the zero-field resonance, which lies at 390 ± 5 GHz, allowing us to estimate the gap Δ as ∼13 cm^{-1}. The simulation parameters were obtained from the 2-D field/frequency map (Figure 5): $|D| = 5.88$ cm^{-1}, $|E| = 1.54$ cm^{-1}, and $\mathbf{g} = [2.21, 2.20, 2.194]$. As attested by Figures S11 and 4, the sign of D is negative.

Quantum-Chemical Calculations. The Co(II) complexes were studied by contemporary *ab initio* methods of quantum chemistry to address the electronic origin of the zfs and support the experimental results. In order to accurately reproduce the experimental conditions, crystallographic geometries were used in these calculations. The results are listed in Table 2, and also visualized in Figure 6, showing a very satisfactory agreement between the experimental and calculated D parameters. The sign of D is consistent with experimental results in all

dx.doi.org/10.1021/ic400980b | Inorg. Chem. 2013, 52, 9409−9417

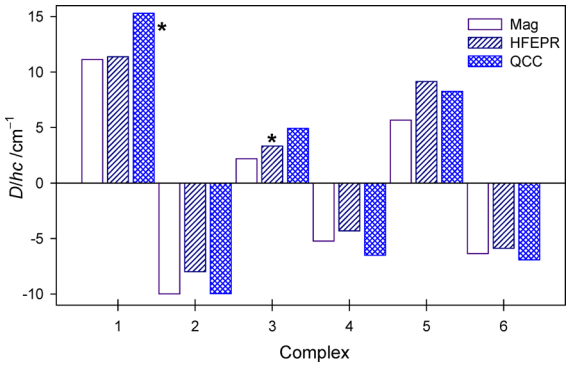

Figure 6. Comparison of the *D* values obtained by different methods. Asterisk denotes situations when a determination of the sign of the *D* parameter is impossible; for these cases, the sign has been assigned according to other methods. Abbreviations: Mag, Magnetometry; HFEPR, High-Frequency and -Field Electron Paramagnetic Resonance; QCC, Quantum-Chemical Calculation.

complexes, except in **1**. However, considering the boundary rhombicity of the *ab-initio*-calculated zfs tensor ($E/D \sim 1/3$), an assignment of the sign is inappropriate in this case.

Neglecting the spin−spin coupling SSC (for the studied systems the SSC contributes only a minor part to the overall *D*), the *D* parameter is the sum of the spin−orbit coupling SOC contributions from excited states involved; therefore, the calculated transition energies of the studied complexes will be reviewed in this section first. Experimental electronic spectra (Figure S12) show two principal d−d bands in the recorded region, i.e. approximately at 9000−10 000 and at 16 000−18 000 cm^{-1}, respectively. The first observed band refers to the $\Delta_2 = {}^4A_2 \rightarrow {}^4T_1(F)$ transition in the idealized T_d symmetry (Figure 7).[20] The second one refers to the $\Delta_3 = {}^4A_2 \rightarrow {}^4T_1(P)$

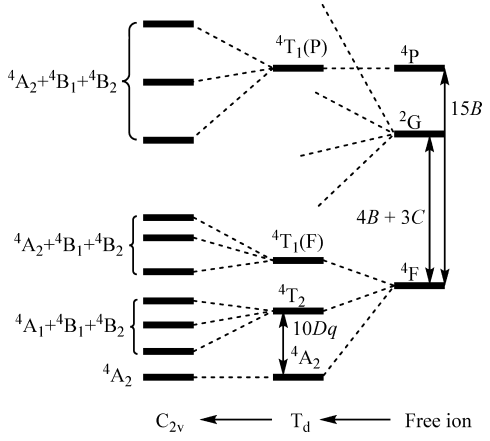

Figure 7. Diagram of crystal-field terms for the pseudotetrahedral Co(II).

transition, which is, however, visibly split. In a more realistic C_{2v} point group, this splitting corresponds to the transitions to ${}^4A_2$, ${}^4B_1$, and ${}^4B_2$ terms, respectively. Thus, there are nine spin-allowed transitions in this effective symmetry, which are complemented by transitions to doublet terms (spin-forbidden transitions are partially allowed by the "intensity-borrowing" mechanism[21]).

Calculated spin-allowed transition energies are summarized in Tables S2 and S3. As seen from Table S2, the CASSCF results show quite large errors, especially for the second observed (Δ_3) d−d band (calculated values shifted up to ∼23 000 cm^{-1}). As discussed elsewhere, this unsatisfactory result is a consequence of overestimating the electronic repulsion.[22] The errors are somewhat reduced by the NEVPT2 method, which is particularly evident for the Δ_2 transitions; for these, the results are comparable with experimental results. However, for the Δ_3 transition, the improvement is not sufficient. The first transitions $\Delta_1 = {}^4A_2 \rightarrow {}^4T_2$ in the region below 9000 cm^{-1} have not been experimentally detected (owing to the hardware limitations, Specord 200, Analytical Jena, 9000−50 000 cm^{-1}). Their CASSCF-calculated values range from 2000 to 4500 cm^{-1} and the inclusion of dynamic correlation effects shifts this interval up to 3000−6000 cm^{-1}.

Individual quartet and doublet contributions to the *D* value are shown in Tables 3, 4, S4, and S5, respectively. For all complexes, the dominant contribution (∼80%) arises from the ${}^4T_2$ excited states; moreover, they define the sign of the *D* parameter. Contributions from the ${}^4T_1(P)$ members are negligible. The doublet terms have significantly less impact on the overall *D* than the quartet terms. The lowest lying ${}^2G$ free ion members lie at ∼22 000 cm^{-1} and contribute the major part of the total doublet effect on the zfs. As can be expected, in the T_d symmetry the most dominant doublet contribution comes from the ${}^2T_2({}^2G)$ term (for example, for complex **2** the contributions are up to 5.6, −2.9, and −2.4 cm^{-1}, respectively). However, these contributions cancel each other; therefore the total doublet-contributed *D* values barely exceed 1 cm^{-1}.

Structural dependence of the zfs has been theoretically studied by wide-range modeling that has been done by means of the generalized crystal-field theory.[12,23] In Figure 8, an angular dependence of the zfs is shown which implies that for flattened pseudotetrahedral symmetries (α and $\beta < 109.47°$) the *D* values are negative and *vice versa*. *Ab initio* calculations confirm this assumption (see Supporting Information, Figure S13). However, confrontation of the model with experimental data reveals a clear discrepancy.

In general, the present study constitutes significant progress in understanding the relationship between the magnetic and electronic properties of the (pseudo)tetrahedral Co(II) coordination complexes. It shows that the early studies in this area[14a] were doomed to fail, being based on both inadequate experimental techniques and simplistic assumptions. The following work[14b] showed some progress in both the instrumental (employing Magnetic Circular Dichroism, MCD) and theoretical (using Angular Overlap Model, AOM) domains, yet the results were still less than satisfactory. More recent research on (pseudo)tetrahedral Co(II)[13a,b] brought the experimental part to the current state-of-the-art yet was still missing a dependable theoretical treatment, which has only become available recently.[14d] Thus, it has only now become possible to combine the armamentaria of both the experimental and calculational methods to study Co(II) in (pseudo)-tetrahedral coordination. And yet, this particular system escapes easy qualitative conclusions as to the magnetostructural correlations, as witnessed by Figure 6: it can be seen that seemingly minute changes in geometry result in drastic changes of magnetic properties such as the sign of *D*. It thus appears that, at least at this stage, only case-by-case QCC calculations on the highest modern level can bring about the desired correlation between the geometric and electronic structure on one side and the magnetic properties on the other.

dx.doi.org/10.1021/ic400980b | Inorg. Chem. 2013, 52, 9409−9417

Table 3. Dominant Quartet States Contributions to the D Parameter (CASSCF/NEVPT2/QDPT) (in cm^{-1})

T_d	1	2	3	4	5	6
$^4T_2(F)$	−35.285	−31.144	0.329	−28.811	10.139	−12.998
	12.633	11.429	3.715	10.954	12.193	5.782
	2.898	9.842	−1.601	11.363	−10.487	2.711
$^4T_1(F)$	3.747	0.232	1.588	0.324	−3.208	1.208
	0.005	0.028	0.025	−0.066	−0.063	0.062
	0.248	−0.280	−0.126	−0.069	−0.247	−0.083
$^4T_1(P)$	0.003	0.005	0.006	0.005	−0.008	−0.009
	0.007	0.000	0.002	0.000	−0.007	0.002
	−0.017	−0.022	−0.012	−0.009	0.004	0.008

Table 4. Dominant Doublet States Contributions to the D Parameter (CASSCF/NEVPT2/QDPT) (in cm^{-1})

T_d	1	2	3	4	5	6
$^2E(G)$	−0.522	−0.259	0.081	−0.196	−0.393	−0.205
	0.410	0.350	0.216	0.027	0.328	0.595
$^2T_1(G)$	−0.017	−0.001	−0.013	0.074	−0.033	−0.025
	0.760	−0.003	−0.114	0.041	−0.233	−0.056
	−0.022	0	−0.061	0.007	−0.099	−0.088
$^2A_1(G)$	−0.073	0	−0.002	−0.002	−0.008	−0.002
$^2T_2(G)$	4.423	5.591	2.463	5.604	−0.563	3.806
	−2.404	−2.959	−0.276	−2.743	−2.033	−2.721
	−1.633	−2.463	−1.053	−2.649	2.41	−0.015

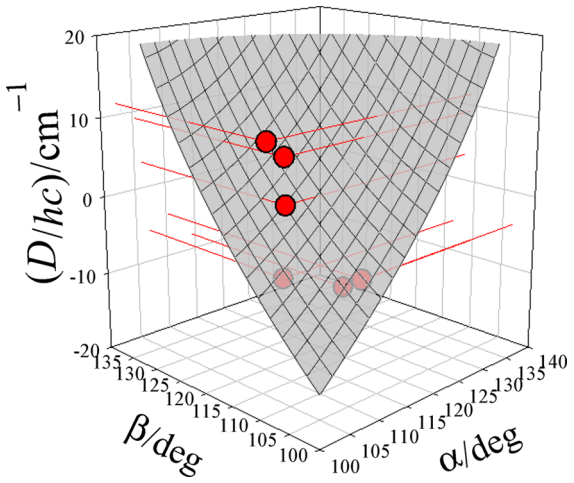

Figure 8. Angular mapping of the zero-field splitting D parameter for pseudotetrahedral Co(II) complexes (surface). All crystal-field poles F_4 = 5000 cm^{-1}, B = 900 cm^{-1}. Circles, experimental data.

CONCLUSIONS

We have combined magnetometric, spectroscopic, and theoretical techniques to determine the zero-field splitting in a series of pseudotetrahedral Co(II) complexes. The coordination sphere of these compounds consists of two N-donor heterocycles completed by two chloro ligands. The $\{CoN_2Cl_2\}$ chromophores exhibit distortions from the ideal C_{2v} pattern that refer to the C_2 and C_1 symmetries, respectively. Intricate angular distortions split the ground crystal-field term $^4A_2$ into crystal-field multiplets that refer to a pair of Kramers doublets $|S,M_S\rangle$; they define the energy gap $\Delta = \varepsilon(|3/2, \pm 3/2\rangle) - \varepsilon(|3/2, \pm 1/2\rangle) = 2(D^2 + 3E^2)^{1/2}$.

The analysis of the HFEPR spectra provides D values that are ranging in the interval of −8 to +11 cm^{-1}. For complexes **1**, **3**, and **5**, the D value is positive, whereas for **2**, **4**, and **6** the D parameter is negative. Magnetometric data are capable of yielding comparable results, however, only after considering some important aspects. First, a comparison of the magnetometric D values obtained in this work with earlier results[10] (when E was neglected) points to a considerable importance of the rhombic term in the spin-Hamiltonian analysis. Furthermore, more emphasis on the field dependence of magnetization in the simultaneous fitting procedure (χ vs T, M vs B) significantly improves the results. Usually the weighing factors in the functional F_2 obey $w(\chi) > w(M)$; in the present case, however, a better choice is $w(\chi) < w(M)$. Overall comparison of the D values from magnetometry, HFEPR measurements, and quantum-chemical calculations is shown in Figure 6. As can be seen, the standard deviation of parameters for a given complex obtained by different methods does not exceed 2 cm^{-1}. The agreement between quantum-chemical calculations and both experimental methods is particularly rewarding. Despite the good consistency of the D parameters obtained by all three main methods, it is not yet possible at this stage of research to formulate a meaningful magnetostructural correlation such as was done previously for hexacoordinate Ni(II). We assume that for the studied complexes the overall structural distortion should be considered through an appropriately designed structural parameter. To this end, a richer collection of reliable experimental data such as those presented in this work is required.

ASSOCIATED CONTENT

Supporting Information

Details of fitting procedure of the magnetic data, complete set of the fitted magnetic parameters, HFEPR spectra obtained using the VDI-based spectrometer, electronic spectra and a diagram of crystal-field terms, and tables of *ab initio* calculation results. This material is available free of charge via the Internet at http://pubs.acs.org.

dx.doi.org/10.1021/ic400980b | Inorg. Chem. 2013, 52, 9409−9417

AUTHOR INFORMATION

Corresponding Author

*E-mail: jan.titis@ucm.sk (J.T.), krzystek@magnet.fsu.edu (J.K.).

Notes

The authors declare no competing financial interest.

ACKNOWLEDGMENTS

Slovak Grant Agencies (VEGA 1/0233/12 and APVV-0014-11) and FPPV-04-2012 are acknowledged for the financial support. Part of the work was performed at the National High Magnetic Field Laboratory, Tallahassee, FL, which is funded by the NSF through Cooperative Agreement DMR 1157490, the State of Florida, and the DOE. M.I. is thankful to the Slovak Academic Information Agency for a stipend covering her stay at the NHMFL. We thank Dr. Andrew Ozarowski for his EPR simulation program SPIN.

REFERENCES

(1) (a) Perlepes, S. P.; Huffman, J. C.; Christou, G. *Polyhedron* **1991**, *10*, 2301. (b) Tokii, T.; Nagamatsu, M.; Hamada, H.; Nakashima, M. *Chem. Lett.* **1992**, 1091. (c) Perlepes, S. P.; Huffman, J. C.; Christou, G.; Paschalidou, S. *Polyhedron* **1995**, *14*, 1073. (d) Rajendiran, T. M.; Kannappan, R.; Venkatesan, R.; Rao, P. S.; Kandaswamy, M. *Polyhedron* **1999**, *18*, 3085. (e) Graham, B.; Hearn, M. T. W.; Junk, P. C.; Kepert, C. M.; Mabbs, F. E.; Moubaraki, B.; Murray, K. S.; Spiccia, L. *Inorg. Chem.* **2001**, *40*, 1536. (f) Huang, W.; Hu, D.; Gou, S.; Qian, H.; Fun, H.-K.; Raj, S. S. S.; Meng, Q. *J. Mol. Struct.* **2003**, *649*, 269. (g) Chadjistamatis, I.; Terzis, A.; Raptopoulou, C. P.; Perlepes, S. P. *Inorg. Chem. Commun.* **2003**, *6*, 1365. (h) Youngme, S.; Phatchimkun, J.; Wannarit, N.; Chaichit, N.; Meejoo, S.; van Albada, G. A.; Reedijk, J. *Polyhedron* **2008**, *27*, 304.

(2) Ruiz, E. *Struct. Bonding (Berlin)* **2004**, *113*, 71.

(3) (a) Gorun, S. M.; Lippard, S. J. *Inorg. Chem.* **1991**, *30*, 1625. (b) Law, N. A.; Kampf, J. W.; Pecoraro, V. L. *Inorg. Chim. Acta* **2000**, *297*, 252.

(4) (a) Boča, R.; Titiš, J. In *Coordination Chemistry Research Progress*; Nova Science Publishers: New York, 2008, pp 247−304. (b) Titiš, J.; Boča, R. *Inorg. Chem.* **2010**, *49*, 3971. (c) Packová, A.; Miklovič, J.; Titiš, J.; Koman, M.; Boča, R. *Inorg. Chem. Commun.* **2013**, *32*, 9.

(5) (a) Titiš, J.; Boča, R. *Inorg. Chem.* **2011**, *50*, 11838. (b) Titiš, J.; Hudák, J.; Kožíšek, J.; Krutošíková, A.; Moncol', J.; Tarabová, D.; Boča, R. *Inorg. Chim. Acta* **2012**, *388*, 106.

(6) Boča, R. *Struct. Bonding (Berlin)* **2006**, *117*, 1.

(7) (a) Papánková, B.; Boča, R.; Dlháň, L'.; Nemec, I.; Titiš, J.; Svoboda, I.; Fuess, H. *Inorg. Chim. Acta* **2010**, *363*, 147. (b) Šebová, M.; Boča, R.; Dlháň, L'.; Nemec, I.; Papánková, B.; Pavlik, J.; Fuess, H. *Inorg. Chim. Acta* **2012**, *383*, 143.

(8) (a) Zadrozny, J. M.; Liu, J.; Piro, N. A.; Chang, C. J.; Hill, S.; Long, J. R. *Chem. Commun.* **2012**, *48*, 3927. (b) Walsby, C. J.; Krepkiy, D.; Petering, D. H.; Hoffman, B. M. *J. Am. Chem. Soc.* **2003**, *125*, 7502. (c) Murrie, M. *Chem. Soc. Rev.* **2010**, *39*, 1986. (d) Zadrozny, J. H.; Long, J. R. *J. Am. Chem. Soc.* **2011**, *133*, 20732. (e) Maganas, D.; Sottini, S.; Kyritsis, P.; Groenen, E. J. J.; Neese, F. *Inorg. Chem.* **2011**, *50*, 8741.

(9) (a) Fukui, F.; Kojima, N.; Ohya-Nishiguchi, H.; Hirota, N. *Inorg. Chem.* **1992**, *31*, 1338. (b) Šebová, M.; Jorík, V.; Kožíšek, J.; Moncol', J.; Boča, R. *Polyhedron* **2011**, *30*, 1163.

(10) Idešicová, M.; Dlháň, L'.; Moncol', J.; Titiš, J.; Boča, R. *Polyhedron* **2012**, *36*, 79.

(11) (a) Davies, J. E.; Gerloch, M.; Phillips, D. J. *J. Chem. Soc., Dalton Trans.* **1979**, 1836. (b) Carlin, R. L.; Chirico, R. D.; Sinn, E.; Mennenga, G.; De Jongh, L. J. *Inorg. Chem.* **1982**, *21*, 2218. (c) Nelson, D.; ter Haar, L. W. *Inorg. Chem.* **1993**, *32*, 182.

(12) Boča, R. A. *Handbook of Magnetochemical Formulae*; Elsevier: Amsterdam, 2012.

(13) (a) Krzystek, J.; Zvyagin, S. A.; Ozarowski, A.; Fiedler, A. T.; Brunold, T. C.; Telser, J. *J. Am. Chem. Soc.* **2004**, *126*, 2148. (b) Krzystek, J.; Swenson, D. C.; Zvyagin, S. A.; Smirnov, D.; Ozarowski, A.; Telser, J. *J. Am. Chem. Soc.* **2010**, *132*, 5241. (c) Krzystek, J.; Ozarowski, A.; Telser, J. *Coord. Chem. Rev.* **2006**, *250*, 2308. (d) Fukui, K.; Ohya-Nishiguchi, H.; Hirota, N. *Bull. Chem. Soc. Jpn.* **1991**, *64*, 1205. (e) Fukui, K.; Masuda, H.; Ohya-Nishiguchi, H.; Kamada, H. *Inorg. Chim. Acta* **1995**, *238*, 73. (f) Maganas, D.; Milikisyants, S.; Rijnbeek, J. M. A.; Sottini, S.; Levesanos, N.; Kyritsis, P.; Groenen, E. J. J. *Inorg. Chem.* **2010**, *49*, 595.

(14) (a) Makinen, M. W.; Kuo, L. C.; Yim, M. B.; Wells, G. B.; Fukuyama, J. M.; Kim, J. E. *J. Am. Chem. Soc.* **1985**, *107*, 5245. (b) Larrabee, J. A.; Alessi, C. M.; Asiedu, E. T.; Cook, J. O.; Hoerning, K. R.; Klingler, L. J.; Okin, G. S.; Santee, S. G.; Volkert, T. L. *J. Am. Chem. Soc.* **1997**, *119*, 4182. (c) Jenkins, D. M.; Peters, J. C. *J. Am. Chem. Soc.* **2005**, *127*, 7148. (d) Sundararajan, M.; Ganyushin, D.; Ye, S.; Neese, F. *Dalton Trans.* **2009**, 6021.

(15) (a) Safronova, L. A.; Komyagin, N. T.; Yanovsky, A. I.; Struchkov, Yu. T.; Shebaldova, A. D. *Koord. Khim.* **1987**, *13*, 1407. (b) Oki, J.; Sanchez, A. R.; Hamilton, S.; Emge, T. J. *J. Coord. Chem.* **1995**, *36*, 63. (c) Guzei, I. A.; Spencer, L. C. Unpublished, 2006. (d) Rosu, T.; Negolu, M.; Strenger, I.; Muller, U. *Z. Anorg. Allg. Chem.* **1977**, *623*, 1201. (e) Pike, R. D.; Jung Lim, Mi; Willcox, E. A. L.; Tronic, T. A. *J. Chem. Cryst.* **2006**, *36*, 781. (f) Yoe-Reyes, F.-J.; Bernes, S.; Barba-Behrens, N. *Acta Crystallogr.* **2005**, *E61*, m875.

(16) Cambridge Crystallographic Data Centre, 12 Union Road, Cambridge CB2 1EZ, U.K. CCDC codes for **1**−**6** (CCDC codes for **1**−**3** re-determined by some of us in ref 9 are in parentheses): RESYUJ (848840), SEQFIE (801981), SAPBIV (848841), VETSOC, DIMZCO, VUWZIW01. http://www.ccdc.cam.ac.uk/conts/retrieving.html.

(17) (a) Boča, R. Program POLYMAGNET, STU Bratislava, 2006. (b) Ozarowski, A. Program SPIN, NHMFL Tallahassee.

(18) (a) Hassan, A. K.; Pardi, L. A.; Krzystek, J.; Sienkiewicz, A.; Goy, P.; Rohrer, M.; Brunel, L. C. *J. Magn. Reson.* **2000**, *142*, 300. (b) Zvyagin, S. A.; Krzystek, J.; van Loosdrecht, P. H. M.; Dhalenne, G.; Revcolevschi, A. *Physica B* **2004**, *346*−*347*, 1.

(19) (a) Neese, F. *ORCA*, version 2.8−20; University of Bonn: Bonn, Germany, 2010. (b) Atanasov, M.; Ganyushin, D.; Pantazis, D. A.; Sivalingam, K.; Neese, F. *Inorg. Chem.* **2011**, *50*, 7460. (c) Angeli, C.; Borini, S.; Cestari, M.; Cimiraglia, R. *J. Chem. Phys.* **2004**, *121*, 4043. (d) Angeli, C.; Cimiraglia, R.; Evangelisti, S.; Leininger, T.; Malrieu, J.-P. *J. Chem. Phys.* **2001**, *114*, 10252. (e) Angeli, C.; Cimiraglia, R.; Malrieu, J.-P. *J. Chem. Phys.* **2002**, *117*, 9138. (f) Neese, F. *J. Chem. Phys.* **2005**, *122*, 34107. (g) Ganyushin, D.; Neese, F. *J. Chem. Phys.* **2006**, *125*, 24103. (h) Neese, F. *J. Chem. Phys.* **2007**, *127*, 164112.

(20) Lever, A. B. P. *Inorganic Electronic Spectroscopy*, 2nd ed.; Elsevier: Amsterdam, 1984.

(21) Figgis, B. N.; Hitchmann, M. A. *Ligand Field Theory and Its Applications*; Wiley: New York, 2000.

(22) Neese, F.; Petrenko, T.; Ganyushin, D.; Olbrich, G. *Coord. Chem. Rev.* **2007**, *251*, 288.

(23) Boča, R.; Herchel, R. Program TERMS, STU Bratislava, 2003.